NANO LETTERS

Letter

pubs.acs.org/NanoLett

Wavelength-Tunable Spasing in the Visible

Xiangeng Meng,*[,†,‡] Alexander V. Kildishev,[‡] Koji Fujita,*[,†] Katsuhisa Tanaka,[†] and Vladimir M. Shalaev*[,‡]

[†]Department of Material Chemistry, Graduate School of Engineering, Kyoto University, Katsura, Nishikyo-ku 615-8510, Kyoto, Japan

[‡]School of Electrical and Computer Engineering and Birck Nanotechnology Center, Purdue University, West Lafayette, Indiana 47907, United States

Supporting Information

ABSTRACT: A SPASER, short for surface plasmon amplification by stimulated emission of radiation, is key to accessing coherent optical fields at the nanoscale. Nevertheless, the realization of a SPASER in the visible range still remains a great challenge because of strong dissipative losses. Here, we demonstrate that room-temperature SPASER emission can be achieved by amplifying longitudinal surface plasmon modes supported in gold nanorods as plasmon nanocavities and utilizing laser dyes to supply optical gain for compensation of plasmon losses. By choosing a particular organic dye and adjusting the doping level, the resonant wavelength of the SPASER emission can be tuned from 562 to 627 nm with a spectral line width narrowed down to 5−11 nm. This work provides a versatile route toward SPASERs at extended wavelength regimes.

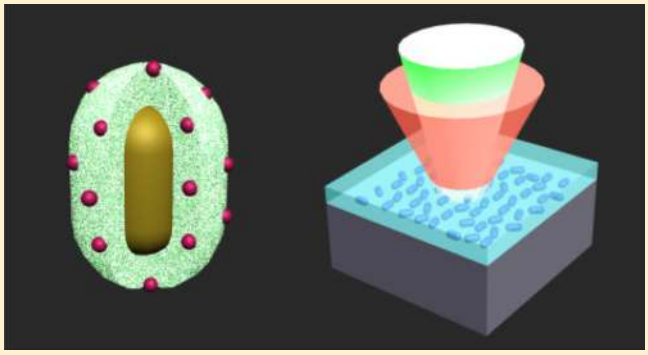

KEYWORDS: *SPASER, gold nanorods, resonant energy transfer, wavelength tunability*

The laser has revolutionized many aspects of modern life, including optical communications, data storage, and biomedicine. The ever-increasing demands for bandwidth and information density in the fields of communications and computing call for on-chip coherent optical sources scaled down to subwavelength dimensions. However, conventional lasers built on dielectric cavities cannot have dimensions smaller than half the optical wavelength due to the diffraction limit of light.[1] This long-standing barrier can be overcome with plasmonic nanocavities that rely on surface plasmons (SPs), which are collective electron oscillations at a metal-dielectric interface. These SP modes can provide feedback on the nanometer scale and open the path to lasing as long as an optical gain medium placed near the metal nanostructure compensates for dissipative losses.[2] This new compact source of coherent light has been named a "SPASER"[2] or a plasmon laser. Since plasmon modes have no cutoff, the SPASER can offer coherent optical fields at truly nanometer scales. This unique capability has attracted wide attention recently,[3−36] resulting in the achievement of several important milestones thus far.

State-of-the-art SPASERs have been achieved through several approaches[15−25] involving the amplification of both propagating surface plasmon polaritons (SPPs) generated in planar structures[15−24] and localized surface plasmons (LSPs) in a nanoparticle geometry.[25] For most SPP-based SPASERs,[15−24] the cavity features a delicate configuration (e.g., Fabry−Perot cavity, distributed feedback cavity, whispering gallery cavity) so as to generate intense SPP feedback for spasing. In contrast, the optical feedback in LSP-based SPASERs arises from the intrinsic plasmon resonance,[25] which provides three-dimensional confinement. A single-particle plasmon nanocavity is of particular interest because it can support an ultrahigh Purcell factor F as a result of ultrasmall mode volume V. Nevertheless, so far there is only one report on an LSP-based SPASER, which consisted of dye-decorated gold-silica core−shell nanoparticles as resonant cavities.[25] In that case, the particles were produced using a modification to the procedure to prepare so-called Cornell quantum dots.[37] Several severe limitations exist in this procedure. First, dye molecules should be capable of being covalently conjugated to the silica precursor through some specific group in the chemical structure of the dye molecule.[37] Unfortunately, commercial laser dyes are rarely compatible with this method due to the absence of a functional group for covalent bonding.[38] Second, the procedure requires stringent fabrication skills to achieve a doping concentration sufficient to compensate plasmon losses. Third, the spectral position of the plasmon mode in a spherical metal structure is difficult to tune when optimizing the energy transfer from the gain material to the metal. This is especially troublesome if other gain materials with different emission lines are to be incorporated into a

Received: May 1, 2013
Revised: July 16, 2013
Published: August 5, 2013

   dx.doi.org/10.1021/nl4015827 | *Nano Lett.* 2013, 13, 4106−4112

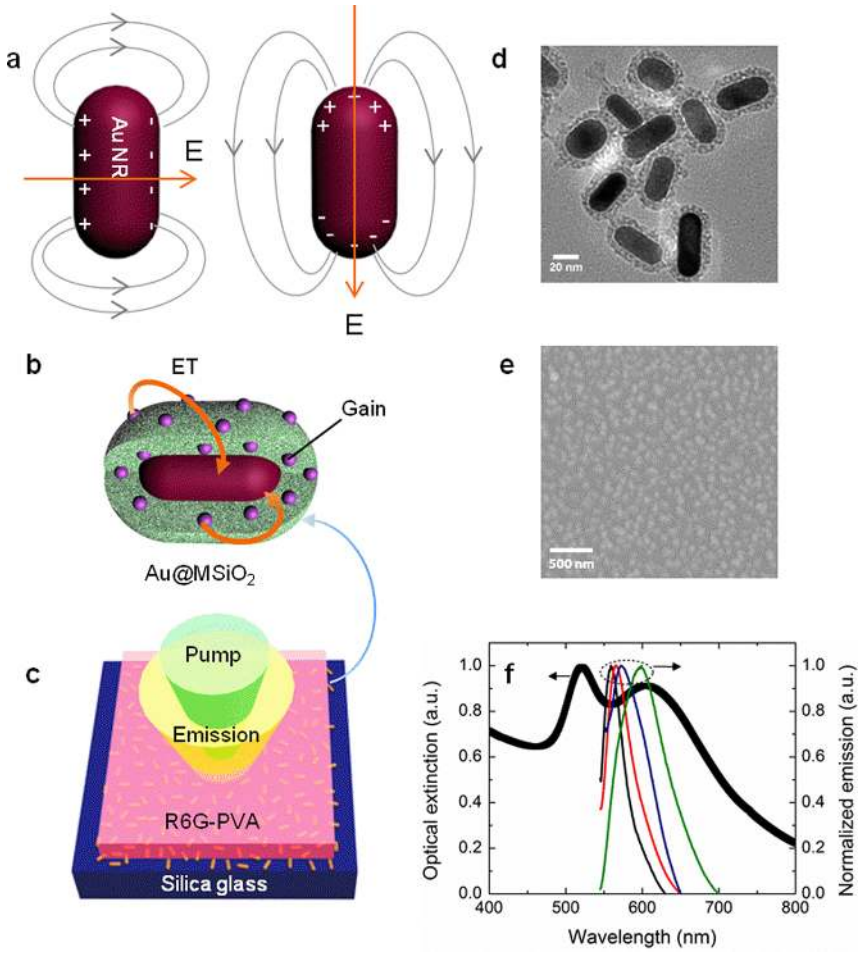

Figure 1. Working principle of the SPASER, excitation-detection scheme, and sample characterizations. (a) An Au NR exhibits transverse (left) and longitudinal (right) SPR modes that are oriented perpendicular and parallel to the long axis, respectively. (b) An Au@$MSiO_2$ NR with optical gain embedded in the mesopores of the silica shell. The molecules are excited with a laser beam and then transfer energy to the Au NR, allowing for the excitation and amplification of surface plasmons. (c) SPASER sample and excitation-detection scheme. The SPASER system consists of a monolayer of Au@$MSiO_2$ NRs covered with a 200 nm thick R6G-PVA film to supply gain. The second-harmonic output of a mode-locked Nd: YAG laser (operation wavelength, 532 nm; pulse duration, 25 ps; repetition rate, 1 Hz) was used as the pump source and was focused to a 1.6 mm diameter spot on the front surface of the sample. The emission was collected around the pump beam. No thermal modifications of Au NRs including their melting have been observed upon laser irradiation since the optical extinction spectra of the SPASER systems remain unchanged after the lasing experiments. The arrows indicate Au@$MSiO_2$ NR particles assembled on the silica substrate. (d) TEM image of Au@$MSiO_2$ NRs. (e) FE-SEM image of a monolayer of Au@$MSiO_2$ NRs. (f) Extinction spectrum of an aqueous suspension of Au NRs (solid squares), and the emission spectra of R6G-PVA at different concentrations: c = 10 (black line), 50 (red line), 100 (navy line), and 200 mM (olive line).

SPASER design later on. These limitations hinder the applicability of LSP-based SPASERs at extended wavelengths.

In this article, we show that wavelength-tunable SPASERs can be achieved in a plasmonic structure composed of a monolayer of mesoporous silica-coated Au nanorods (Au@$MSiO_2$ NRs) as plasmonic nanocavities and organic laser dyes as optical gain media. By changing either the doping level or the chemical composition of the laser dye, we demonstrate the experimental realization of SPASERs with resonance wavelengths ranging from 562 to 627 nm and with spectral linewidths narrowed down to 5−11 nm. By comparing our emission with random lasing in systems constructed with dielectric particles, we exclude the role of light scattering in the onset of SPASERs. Our calculations suggest that the optical gain supplied in our SPASER systems is sufficient to compensate for plasmon losses. Moreover, our 3D numerical simulations indicate that the nanorod cavity supports an ultrasmall V to achieve an ultrahigh F ($\sim 10^4$) despite an inherently low quality factor Q. This class of SPASERs can operate at a moderate gain level, and therefore, a large range of gain materials is suitable for fabricating SPASERs operating in a broad wavelength band.

The system we investigate here consists of a monolayer of randomly oriented Au@$MSiO_2$ NRs. The core−shell NRs are dispersed on a silica glass substrate and then covered by a polyvinyl alcohol (PVA) thin film embedded with highly fluorescent rhodamine 6G (R6G) molecules that serve as the optical gain (Figure 1c). We use Au NRs because they support both transverse and longitudinal surface plasmon resonance (SPR) modes (Figure 1a), and the longitudinal modes are believed to provide low-threshold SP excitation.[39] The longitudinal modes support higher local field enhancement than the transverse modes (Supporting Information Figure S1), and therefore can provide a stronger optical feedback for spasing. The sample design contains the following two important features: (i) embedding the dye in a polymer host, and (ii) encapsulation of the Au NRs with mesoporous silica shells. Embedding the dye into a polymer host improves the

dx.doi.org/10.1021/nl4015827 | Nano Lett. 2013, 13, 4106−4112

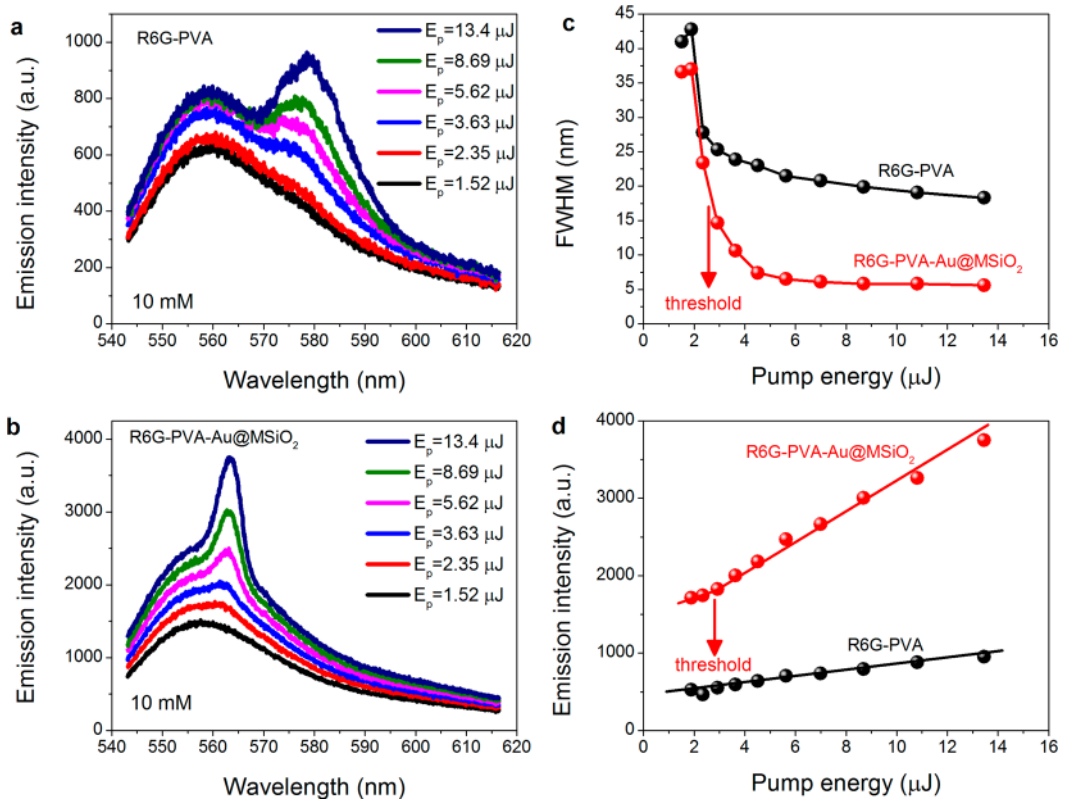

Figure 2. ASE in R6G-PVA and spasing in R6G-PVA-Au@$MSiO_2$. (a,b) Evolution of emission spectra with E_p for R6G-PVA (a) and R6G-PVA-Au@$MSiO_2$ (b): c = 10 mM. The emission spectra were recorded under equivalent excitation and detection conditions. (c) E_p dependence for the fwhm and (d) peak ASE intensity from R6G-PVA (black) and SPASER from R6G-PVA-Au@$MSiO_2$ (red). The arrows indicate the pump threshold for SPASER emission to occur. A clear threshold behavior is not manifested in ASE, likely because of its rather weak signal.

dye photostability and efficiently reduces fluorescence self-quenching of the dye. The silica coating provides easy self-assembly of particles on the glass substrate. In contrast, the arrangement of bare Au NRs on a glass substrate requires additional surface modification of the particles from which large clusters easily form.[40] Compared with a solid silica shell, the mesoporous shell structure makes it possible to surround the Au NR with optical gain media by caging the optical gain inclusions inside the mesoscopic pores, therefore allowing for efficient energy transfer (ET) from the gain material to the Au NR (Figure 1b).

The transmission electron microscopy (TEM) image shows that the diameter and length of the Au NRs, as well as the shell thickness of SiO_2, are 20 ± 8, 40 ± 20, and 10 ± 1 nm (Figure 1d), respectively. These Au NRs have a broad size distribution (Supporting Information Figure S2). The field-emission scanning electron microscopy (FE-SEM) image shows a monolayer distribution of the Au@$MSiO_2$ NRs (Figure 1e), from which the areal density of the Au@$MSiO_2$ NRs is evaluated to be 1.6×10^7 mm^{-2}. As shown in Figure 1f, the SPR spectrum of the monolayer of Au@$MSiO_2$ NRs consists of two peaks centered around λ = 520 and 610 nm due to the transverse and longitudinal modes, respectively. The longitudinal SPR mode is very sensitive to the aspect ratio of the NR, as illustrated in our simulations (Supporting Information Figure S3). This dependence and the dispersion of the NR sizes cause the evident broadening of the SPR spectrum in our sample. The emission spectrum of R6G-PVA matches the SPR spectrum, which allows for efficient plasmon-dye coupling (Figure 1f).

To simplify and clarify the sample descriptions, the SPASER system with a dye-doped polymer layer and Au@$MSiO_2$ NRs is referred to as R6G-PVA-Au@$MSiO_2$ in this work. The reference sample with no metal particles in the same dye-doped polymer layer is denoted as R6G-PVA. Figure 2 depicts the evolution of the emission properties for both R6G-PVA and R6G-PVA-Au@$MSiO_2$. The concentration of R6G in the PVA host is c = 10 mM. R6G-PVA exhibits a new emission band centered at λ = 580 nm with increasing pump energy E_p. This band shows a red shift of about 20 nm with respect to the spontaneous emission (SE) peak. Because there is no plasmonic effect involved in the emission of R6G-PVA, the band centered at λ = 580 nm can be distinguished as a signature for amplified spontaneous emission (ASE) from bare R6G. The large red shift stems from the self-absorption of R6G emission.[41] The self-absorption effect is especially obvious for optical species with a large overlap between the optical absorption and emission. In contrast, R6G-PVA-Au@$MSiO_2$ exhibits a new emission band centered at λ = 562 nm with increasing E_p (Figure 2b). The resonant wavelength of the SPASER emission is expected to occur around the maximum of the gain spectrum since SPASER results from the ET process from excited fluorophores to the resonant metallic nanostructures.[31] This has been experimentally demonstrated in the SPASER constructed with core−shell nanoparticles.[25] The new band observed in R6G-PVA-Au@$MSiO_2$ occurs near the SE peak and is therefore consistent with the above-mentioned principle for SPASER. To further distinguish between the two emission bands centered at λ = 580 and 562 nm, we fitted each spectrum in several sub-bands using a set of Lorentzian

dx.doi.org/10.1021/nl4015827 | Nano Lett. 2013, 13, 4106−4112

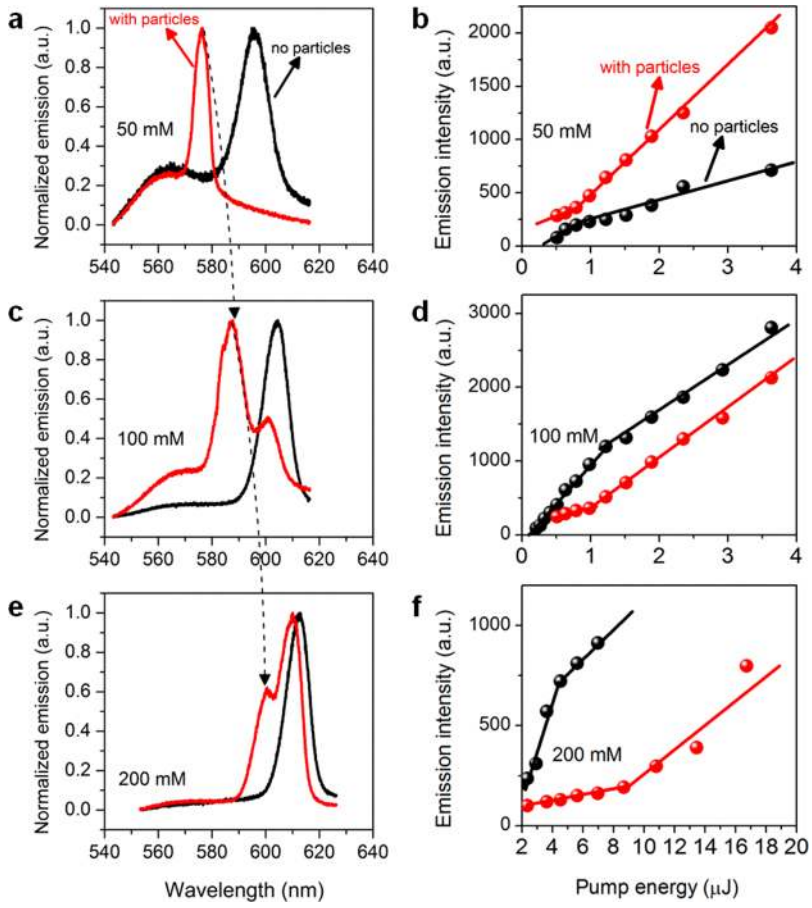

Figure 3. Lasing properties at various c values. (a,c,e) Emission spectra for R6G-PVA (black) and R6G-PVA-Au@$MSiO_2$ (red). The emission spectra were recorded under equivalent excitation and detection conditions. E_p = 3.6 μJ in (a,c), and E_p = 8.7 μJ in (e). The SPASER emission occurs at higher pump threshold for c = 200 mM due to fluorescence quenching. The dotted arrows indicate the evolution of the peak position of SPASER emission with varying c. (b,d,f) E_p-dependence of the emission intensity. The doping concentration is c = 50 (a,b), 100 (c,d), and 200 mM (e,f). The circles in (b,d,f) are experimental data for ASE from R6G-PVA (black) and SPASER emission from R6G-PVA-Au@$MSiO_2$ (red), while the solid lines are guided to eyes.

oscillators in order to separate the corresponding emission bands from the broad spectral background (Supporting Information Figure S4). The full widths at half-maximum (fwhm) of the two emission bands are plotted in Figure 2c as a function of E_p. In the band at λ = 562 nm, the fwhm rapidly decreases down to 5.6 nm as E_p increases. This is in sharp contrast to the situation in the band at λ = 580 nm, which shows a slow decline in fwhm until a value of 18.3 nm is reached. Moreover, the emission at λ = 562 nm is much stronger than that at λ = 580 nm, as shown in Figure 2d. The clear differences manifested in the spectral positions, fwhm values, and emission intensities indicate that there are different origins for these two bands. As follows from these and further considerations, the narrow band centered at λ = 562 nm represents the SPASER emission.

The emergence of SPASER emission near the SE peak offers two feasible ways to tune the resonant wavelength in a given SPASER design: (i) choosing an organic dye with an appropriate emission line shape, and (ii) changing the dye concentration. The latter method is built on the observation that the fluorescence peak red shifts with increasing dye concentration c.[42] Consequently, a corresponding red shift is expected in the SPASER emission. Figure 3 shows the evolution of the emission profile with c for R6G-PVA-Au@$MSiO_2$ when E_p goes beyond a critical value. A narrow emission peak centered at λ = 576 nm emerges in R6G-PVA-Au@$MSiO_2$ (c = 50 mM), while a much broader band centered at λ = 596 nm appears in R6G-PVA (c = 50 mM), as shown in Figure 3a. The 576 nm peak emerges near the SE peak and matches the mechanism of SPASER emission.[31] In contrast, the 596 nm peak shows a large red shift of 35 nm relative to the SE peak. Similar to the situation in R6G-PVA at c = 10 mM, the emission band centered at λ = 596 nm is ascribed to ASE from bare R6G, and the large red shift comes from the self-absorption of R6G emission.[40] In this case, the red shift of ASE peak relative to the SE peak is larger than that observed at c = 10 mM, which we attribute to the increased self-absorption effect at higher dye concentrations.[43] The SPASER emission observed at c = 50 mM exhibits a red shift of 14 nm compared to that observed at c = 10 mM (Figure 2b), which is associated with the red shift in the SE peak as c is increased from 10 to 50 mM.[31] As we increase c further for the R6G-PVA-Au@$MSiO_2$ system up to 100 mM (Figure 3c) and 200 mM (Figure 3e), two new emission peaks appear at the long-wavelength side of the SE peak. The two peaks are observed at λ = 587 and 601 nm for c = 100 mM (red curve, Figure 3c), while the peaks are located at λ = 600 and 610 nm for c = 200 mM (red curve, Figure 3e). This is in contrast to the observation of a single new peak at c = 10 and 50 mM (Figure 3a). Because R6G-PVA exhibits a new peak with a spectral position similar to the long-wavelength

dx.doi.org/10.1021/nl4015827 | Nano Lett. 2013, 13, 4106−4112

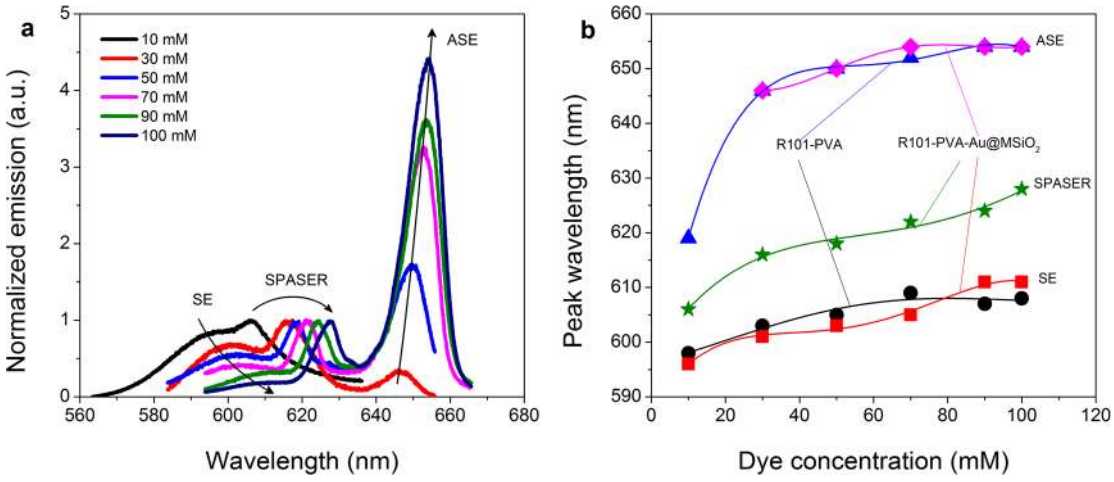

Figure 4. Spasing in R101-PVA-Au@$MSiO_2$. (a) Evolution of emission spectra of R101-PVA-Au@$MSiO_2$ with varying c: 10 (black), 30 (red), 50 (blue), 70 (magenta), 90 (olive), and 100 mM (navy). Each spectrum was normalized to the peak of the SPASER emission. The arrows show the evolution of the peak wavelengths of SE, ASE, and SPASER. (b) Dependence of peak wavelengths of SE, ASE, and SPASER on the gain concentration ranging from 10 to 100 mM.

component of the two new peaks observed in R6G-PVA-Au@$MSiO_2$ (Figure 3c,e), we can attribute the long-wavelength component in R6G-PVA-Au@$MSiO_2$ (c = 100, 200 mM) to ASE from R6G. The short-wavelength component appears near the SE peak and coincides well with the SPASER emission. The appearance of dual peaks composed of SPASER emission and ASE should arise from gain saturation. Figure 3b,d,f shows the dependence of the emission intensity on E_p for the SPASER emission from R6G-PVA-Au@$MSiO_2$ and ASE from R6G-PVA, where a threshold behavior can be clearly identified for the SPASER emission. The SPASER emission is stronger than ASE at c = 50 mM but becomes weaker than ASE when $c \geq 100$ mM. Again, this should arise from gain saturation. Also, a higher threshold was observed when $c \geq 100$ mM, primarily because high levels of optical gain make it difficult for the pump pulse to propagate to the surface of Au NRs.[26]

The fwhm values of the SPASER emission peaks centered at λ = 576, 587, and 600 nm were estimated to be 5.7, 9.2, and 10.8 nm, respectively. The broadening of the SPASER spectrum at higher c is perhaps related to higher losses when the SPASER emission red shifts from 562 to 600 nm (Figure 1f). We note that the fwhm values in refs 14, 19, and 20 are in the range of 1.0 nm or less, much narrower than those reported in this work. This is because our sample is an open system where the optical feedback is not as strong as that provided in SPP-based SPASERs with delicate cavity features (e.g., Fabry–Perot cavities, distributed feedback cavities, whispering gallery cavities). In addition, the broad size distribution of Au NRs as well as the intense fluorescence background may lead to the broadening of the SPASER spectrum. On the other hand, the widths measured here are comparable to the fwhm value in the LSP-based SPASER.[25] They are also similar to the fwhm noted in random lasers with incoherent feedback.[44] The spasing resonance occurs even for c as low as 10 mM in this work, corresponding to a gain coefficient of $g = 1.2 \times 10^3$ cm^{-1}.[45] This is approximately 1 order of magnitude lower than that in ref 25, even though the linewidths are comparable in these two cases.

In an optical system containing randomly dispersed particles, light scattering by particles may elongate the residual time of photons before they escape the system and then lead to light amplification. This is known as the primary mechanism responsible for random lasing. To examine the effects of light scattering and to distinguish our lasing from random lasing, we designed a random lasing system by self-assembling SiO_2 particles on a glass substrate and then covering the particles with a thin layer of dye–polymer film. The resulting system is denoted as R6G-PVA-SiO_2. It should be noted that the scattering strength of R6G-PVA-SiO_2 is designed to be comparable to that of R6G-PVA-Au@$MSiO_2$. We found that the emission properties of R6G-PVA-SiO_2 are distinct from those of R6G-PVA-Au@$MSiO_2$ (Supporting Information Figure S5). At c = 10 mM, no lasing was observed for R6G-PVA-SiO_2, while at $c \geq 50$ mM, only a single peak occurs, and there is no observation of double peaks related to the gain saturation as displayed in R6G-PVA-Au@$MSiO_2$ (Figure 3c,e). The resonant wavelength for R6G-PVA-SiO_2 is quite different from that for R6G-PVA-Au@$MSiO_2$, and the spectral line width of the former is broader than that of the latter. The apparent differences observed between these two systems provide strong evidence that excludes the role of light scattering in the onset of lasing for R6G-PVA-Au@$MSiO_2$. Moreover, we have tried to examine the emission properties of R6G-PVA-Au@$MSiO_2$ when the pump beam was focused to form a pump stripe on the sample. We found that the laser emission was not focused at the end of the pump stripe, instead, the emission has a comparable efficiency around the pump stripe. This clearly suggests that the current lasing is distinct from ASE supported in optical waveguide structure.[46] Our numerical simulations indicate that the optical gain supplied in R6G-PVA-Au@$MSiO_2$ is sufficient to compensate for plasmon losses (Supporting Information Figure S6), therefore supporting the occurrence of spasing.

Changing the doping level in order to tune the resonance wavelength of SPASERs is restricted by the concentration-dependent fluorescence properties of the gain material. A more general way of tuning the wavelength of SPASERs is to use optical gain media with different emission lines. To verify this possibility, we replaced R6G with rhodamine 101 (R101) as the optical gain medium and examined the stimulated emission properties of our samples. The areal density of Au@$MSiO_2$ NRs and the thickness of R101-PVA are $\sim 1.6 \times 10^7$ mm^{-2} and

dx.doi.org/10.1021/nl4015827 | Nano Lett. 2013, 13, 4106–4112

200 nm, respectively. The optical properties of R101 are apparently different from those of R6G (Supporting Information Figure S7), though they both belong to the same family of rhodamine dyes. To clearly distinguish between ASE from bare R101 and SPASERs, we investigated and compared the doping concentration-dependent emission properties for both R101-PVA and R101-PVA-Au@$MSiO_2$. The definitions of R101-PVA and R101-PVA-Au@$MSiO_2$ correspond directly to those of the R6G-based systems. Figure 4a depicts the evolution of the emission spectrum with c ranging from 10 to 100 mM for R101-PVA-Au@$MSiO_2$. The emission properties of R101-PVA-Au@$MSiO_2$ exhibit some similarities to those of R6G-based systems, although some notable differences do exist. At a low concentration (c = 10 mM), R101-PVA-Au@$MSiO_2$ exhibits a new emission band near the SE peak when E_p reaches a critical value, while R101-PVA shows a new emission band with a very large red shift (~21 nm) relative to the SE peak (Supporting Information Figure S8a). The former agrees well with SPASER emission, while the latter case can be ascribed to ASE of bare R101 where the red shift relative to the SE peak is caused by self-absorption of R101 emission. When $c \geq 30$ mM, two new emission bands were observed in R101-PVA-Au@$MSiO_2$ at the long-wavelength side of the SE peak, resembling those observed in R6G-based systems at c = 100 and 200 mM (Figure 3c,e). Since the long-wavelength component of the two new emission bands also appears in R101-PVA, we can attribute it to ASE from R101. However, the short-wavelength component of the two new emission bands is not observed in R101-PVA; in R101-PVA-Au@$MSiO_2$, this component occurs near the SE peak and red shifts along with the SE peak when c increases (Supporting Information Figure S8). We can therefore unambiguously attribute this short-wavelength component to SPASER emission. Note that, in contrast to R6G-PVA-Au@$MSiO_2$, the SE and SPASER emission peaks are sufficiently separated in frequency in R101-PVA-Au@$MSiO_2$ so that these two peaks are well distinguished. The resonant wavelength of the SPASER emission observed in R101-PVA-Au@$MSiO_2$ is tunable from λ = 605 to 627 nm when c is varied from 10 to 100 mM. The differences in the peak spectral positions between the SPASER and ASE components are rather large for R101-PVA-Au@$MSiO_2$, ranging from 28 to 30 nm. This is in contrast to the smaller differences observed in the R6G-based systems (10−14 nm, extracted from Figures 2 and 3). For a clearer illustration of this situation, in Figure 4b we have plotted the gain-level dependences of the peak spectral positions for SE, ASE, and SPASER emission.

The SPASER can be characterized by a range of parameters, such as the quality factor Q, the mode volume V, and the Purcell factor F.[47] Although Q is inherently low for a cavity based on a metal particle because of high losses, F can be comparable to that of high-Q dielectric modes due to the extremely small V far beyond the diffraction limit. Figure 5 depicts the wavelength-dependent V and F for both transverse and longitudinal SPR modes for R6G-PVA-Au@$MSiO_2$ with c = 100 mM. The V values are smaller and F values are higher for the longitudinal modes than for the transverse modes (Figure 5). This might arise from the tighter confinement and higher enhancement of the local fields for the longitudinal SPR mode (Supporting Information Figure S1). This then suggests that the longitudinal SPR modes are more efficient in spasing than the transverse modes. The V value is calculated to be 5.05 × 10^{-24} m^3 at the resonant wavelength λ = 587 nm for the longitudinal modes. The effective mode volume V_{eff} = 8.77 × 10^{-5} $(\lambda/n_{eff})^3$, where n_{eff} = 1.52 is the refractive index of the host. Such an ultrasmall mode volume yields a very high Purcell factor of 2.18 × 10^4. We note that in SPP-based SPASERs, only a moderate F (<100) is observed because of the relatively large V.[14,19,20] The threshold can be expected to be reduced further if plasmon nanostructures with a higher degree of confinement and enhancement are used in SPASERs.

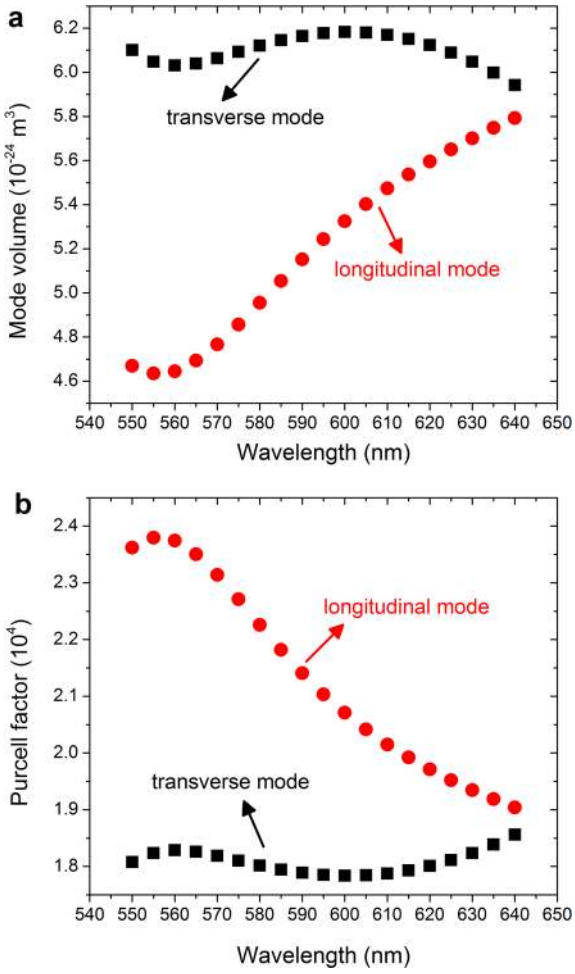

Figure 5. Calculation of the figure of merit for the nanorod cavity. (a,b) Wavelength-dependent mode volume (a) and Purcell factor (b). The sample is R6G-PVA-Au@$MSiO_2$ with c = 100 mM: the transverse mode (solid squares) and longitudinal mode (solid circles).

In our studies, we were also able to observe SPASER emissions even for g < 1.2 × 10^3 cm^{-1}; however, spasing in this case appeared at a much higher pump energy under which the polymer was easily damaged by the intense pump laser pulse. If the host material of the optical gain medium were more tolerant to high-power laser irradiation than the present polymer material, the level of optical gain to reach spasing could be reduced further. The low-threshold behavior of this system means that various optical gain materials (e.g., rare-earth ions, semiconductor quantum dots, and laser dyes) are suitable for spasing. Hence, there is strong potential for the development of SPASERs at extended wavelengths if we simply employ optical gain materials that emit in different parts of the wavelength region. Note that Au@$MSiO_2$ NRs can be assembled on silicon and transparent conducting oxide thin films. Therefore, these designs show promise for the generation

dx.doi.org/10.1021/nl4015827 | Nano Lett. 2013, 13, 4106−4112

of electrically driven subwavelength SPASERs for future photonic circuits.

■ ASSOCIATED CONTENT

Supporting Information

Additional information and figures. This material is available free of charge via the Internet at http://pubs.acs.org.

■ AUTHOR INFORMATION

Corresponding Author

*E-mail: meng14@purdue.edu (X.M.); fujita@dipole7.kuic.kyoto-u.ac.jp (K.F.); shalaev@ecn.purdue.edu (V.M.S).

Notes

The authors declare no competing financial interest.

■ ACKNOWLEDGMENTS

This work was supported in part by Air Force Office of Scientific Research Grant (FA9550-10-1-0264), National Science Foundation Grant (DMR-1120923), NSF "Meta-PREM" Grant (1205457), Office of Navy Research Grant (MURI N00014-13-0649), and by grant in-Aid for Scientific Research B (24350104) and for Challenging Exploratory Research (24656385) from MEXT, Japan. X.M. thanks financial support from Young Researcher Overseas Visits Program for Vitalizing Brain Circulation of JSPS, Japan.

■ REFERENCES

(1) Walther, C.; Scalari, G.; Amanti, M. I.; Beck, M.; Faist, J. *Science* **2010**, *327*, 1495−1497.

(2) Bergman, D. J.; Stockman, M. I. *Phys. Rev. Lett.* **2003**, *90*, 027402.

(3) Seidel, J.; Grafström, S.; Eng, L. *Phys. Rev. Lett.* **2005**, *94*, 177401.

(4) Noginov, M. A.; Zhu, G.; Mayy, M.; Ritzo, B. A.; Noginova, N.; Podolskiy, V. A. *Phys. Rev. Lett.* **2008**, *101*, 226806.

(5) Maier, S. A. *Opt. Commun.* **2006**, *258*, 295−299.

(6) Winter, G.; Wedge, S.; Barnes, W. L. *New J. Phys.* **2006**, *8*, 125.

(7) Gordon, J. A.; Ziokowski, R. W. *Opt. Express* **2007**, *15*, 2622−2653.

(8) Okamoto, T.; Simonen, J.; Kawata, S. *Phys. Rev. B* **2008**, *77*, 115425.

(9) Kumar, P.; Tripathi, V. K.; Liu, C. S. *J. Appl. Phys.* **2008**, *104*, 033306.

(10) Wegner, M.; García-Pomar, J. L.; Soukoulis, C. M.; Meinzer, N.; Ruther, M.; Linden, S. *Opt. Express* **2008**, *16*, 19785−19798.

(11) Zheludev, N. I.; Prosvirnin, S. L.; Papasimakis, N.; Fedotov, V. A. *Nat. Photonics* **2008**, *2*, 351−354.

(12) Ambati, M.; Nam, S. H.; Ulin-Avila, E.; Genov, D. A.; Bartal, G.; Zhang, X. *Nano Lett.* **2008**, *8*, 3998−4001.

(13) Oulton, R. F.; Sorger, V. J.; Genov, D. A.; Pile, D. F. P.; Zhang, X. *Nat. Photonics* **2008**, *2*, 496−500.

(14) Meng, X.; Guler, U.; Kildishev, A. K.; Fujita, K.; Tanaka, K.; Shalaev, V. M. *Sci. Rep.* **2013**, *3*, 1241.

(15) Hill, M. T.; Oei, Y.; Smalbrugge, B.; Zhu, Y.; de Vries, T.; van Veldhoven, P. J.; van Otten, F. W. M.; Eijkemans, T. J.; Turkiewicz, J. P.; de Waardt, H.; Geluk, E. J.; Kwon, S.; Lee, Y.; Nötzel, R.; Smit, M. K. *Nat. Photonics* **2007**, *1*, 589−594.

(16) Hill, M. T.; Marell, M.; Leong, E. S. P.; Smalbrugge, B.; Zhu, Y.; Sun, M.; van Veldhoven, P. J.; Geluk, E. J.; Karouta, F.; Oei, Y.; Nötzel, R.; Ning, C.; Smit, M. K. *Opt. Express* **2009**, *17*, 11107−11112.

(17) Ding, K.; Liu, Z. C.; Yin, L. J.; Hill, M. T.; Marell, M. J. H.; van Veldhoven, P. J.; Noetzel, R.; Ning, C. *Phys. Rev. B* **2012**, *85*, 041301.

(18) Nezhad, M. P.; Simic, A.; Bondarenko, O.; Slutsky, B.; Mizrahi, A.; Feng, L.; Lomakin, V.; Fainman, Y. *Nat. Photonics* **2010**, *4*, 395−3999.

(19) Khajavikhan, M.; Simic, A.; Lee, J. H.; Slutsky, B.; Mizrahi, A.; Lomakin, V.; Fainman, Y. *Nature* **2012**, *482*, 204−207.

(20) Oulton, R. F.; Sorger, V. J.; Zentgraf, T.; Ma, R.; Gladden, C.; Dai, L.; Bartal, G.; Zhang, X. *Nature* **2009**, *461*, 629−632.

(21) Ma, R.; Oulton, R. F.; Sorger, V. J.; Bartal, G.; Zhang, X. *Nat. Mater.* **2011**, *10*, 110−113.

(22) Gather, M. C.; Meerholz, K.; Danz, N.; Leosseon, K. *Nat. Photonics* **2010**, *4*, 457−461.

(23) De Leon, I.; Berini, P. *Nat. Photonics* **2010**, *4*, 382−387.

(24) Lu, Y. J.; Kim, J.; Chen, H. Y.; Wu, C.; Dabidian, N.; Sanders, C. E.; Wang, C. Y.; Lu, M. Y.; Li, B. H.; Qiu, X.; Chang, W. H.; Chen, L. J.; Shvets, G.; Shih, C. K.; Gwo, S. *Science* **2012**, *337*, 450−453.

(25) Noginov, M. A.; Zhu, G.; Belgrave, A. M.; Bakker, R.; Shalaev, V. M.; Narimanov, E. E.; Stout, S.; Herz, E.; Suteewong, T.; Wiesner, U. *Nature* **2009**, *460*, 1110−1113.

(26) Berini, P.; De Leon, I. *Nat. Photonics* **2012**, *6*, 16−24.

(27) Xiao, S.; Drachev, V. P.; Kildishev, A. V.; Ni, X.; Chettiar, U. K.; Yuan, H.; Shalaev, V. M. *Nature* **2010**, *466*, 735−738.

(28) Wuestner, S.; Pusch, A.; Tsakmakidis, K. L.; Hamm, J. M.; Hess, O. *Phys. Rev. Lett.* **2010**, *105*, 127401.

(29) Banerjee, A.; Li, R.; Grebel, H. *Appl. Phys. Lett.* **2009**, *95*, 251106.

(30) Radko, I. P.; Nielsen, M. G.; Albrektsen, O.; Bozhevolnyi, S. I. *Opt. Express* **2010**, *18*, 18633−18641.

(31) Stockman, M. I. *J. Opt.* **2010**, *12*, 024004.

(32) Stockman, M. I. *Phys. Rev. Lett.* **2011**, *106*, 156802.

(33) Chen, Y.; Li, J.; Ren, M.; Wang, B.; Fu, J.; Liu, S.; Li, Z. *Appl. Phys. Lett.* **2011**, *98*, 261912.

(34) Sorger, V. J.; Zhang, X. *Science* **2011**, *333*, 709−710.

(35) Flynn, R. A.; Kim, C. S.; Vurgaftman, I.; Kim, M.; Meyer, J. R.; Mäkinen, A. J.; Bussmann, K.; Cheng, L.; Choa, F. -S.; Long, J. P. *Opt. Express* **2011**, *19*, 8954−8961.

(36) Saleh, A.; Dionne, J. *Phys. Rev. B* **2012**, *85*, 045407.

(37) Ow, H.; Larson, D. R.; Srivastava, M.; Baird, B. A.; Webb, W. W.; Wiersner, U. *Nano Lett.* **2012**, *5*, 113−117.

(38) Duarte, F. J.; Hillman, L. W. *Dye Laser Principle*; Academic: New York, 1990.

(39) Sönnichsen, C.; Franzl, T.; Wilk, T.; von Plessen, G.; Feldmann, J. *Phys. Rev. Lett.* **2002**, *88*, 077402.

(40) Vial, S.; Pastoriza-Santos, I.; Pérez-Juste, J.; Liz-Marzán, L. M. *Langmuir* **2007**, *23*, 4606−4611.

(41) Sorek, Y.; Reisfeld, R.; Finkelstein, I.; Ruschin, S. *Opt. Mater.* **1994**, *4*, 99−101.

(42) Hungerford, G.; Suhling, K.; Ferreira, J. A. *J Photochem. Photobiol. A: Chem.* **1999**, *129*, 71−80.

(43) Taneja, L.; Sharma, A. K.; Singh, R. D. *J. Lumin.* **1995**, *63*, 203−214.

(44) The gain coefficient is evaluated by using $g = \rho\sigma_{em}$, where ρ and σ_{em} represent the density and emission cross section of optical gain, respectively. Thus we obtain $g \sim 1.2 \times 10^3$ cm^{-1} by using $\rho = 6.02 \times 10^{18}$ cm^{-3} (which corresponds to c = 10 mM) and $\sigma_{em} = 2 \times 10^{-16}$ cm^2. Likewise, the threshold gain in ref 25 was found to be $g \sim 1.2 \times 10^4$ cm^{-1} by using $\rho = 4.63 \times 10^{19}$ cm^{-3} and $\sigma_{em} = 2.55 \times 10^{-16}$ cm^2.

(45) Gottardo, S.; Sapienza, R.; García, P. D.; Blanco, A.; Wiersma, D. S.; López, C. *Nat. Photonics* **2008**, *2*, 429−432.

(46) Peng, X.; Liu, L.; Wu, J.; Li, Y.; Hou, Z.; Xu, L.; Wang, W.; Li, F. *Opt. Lett.* **2000**, *25*, 314−316.

(47) Purcell, E. M. *Phys. Rev.* **1946**, *69*, 681.